Journal of Physics: Conference Series **2752** (2024) 012164 doi:10.1088/1742-6596/2752/1/012164

On the Water Jet Quality at Part-Load Operation of Pelton turbines

Bernhard Semlitsch
TU Wien, Getreidemarkt 9/BA, Vienna 1060, Austria
E-mail: bernhard.semlitsch@tuwien.ac.at

Abstract. Pelton turbines with multiple nozzles are characterised by their excellent performance over a wide operating range of mass flow rates. Thus, Pelton turbine manifolds must also be designed to deliver good flow quality to the nozzles at part-load operating conditions to accomplish the expectations. A reduced number of nozzles are opened at low mass flow rate operating conditions, where the choice of the open nozzles depends on the water jet quality generated at the individual nozzles. We investigate the flow phenomena occurring in the manifold with the operation of a reduced nozzle number employing numerical simulations to analyse beneficial nozzle opening selections. The turbulent two-phase flow is predicted by the Volume-Of-Fluid (VOF) approach and the $k-\omega$ SST turbulence closure model. Different nozzle operating scenarios are simulated, and the implications on the water jet quality, i.e. deviation and shape deformation, are reported. The results show that the free water jet quality criteria can change drastically at individual nozzle operating conditions because of the velocity changes at the branch line junctions.

1. Introduction

In contrast to run-of-river systems where restriction of the flow rates has limitations, the flow rates can be adjusted with water reservoirs to balance electricity demand fluctuations. Pelton turbines are commonly used to electrify the potential energy stored in high-altitude water reservoirs [1]. The potential energy is converted into kinetic energy in the form of high-velocity jets at the nozzles. The emerging high-velocity water jets strike the buckets mounted on a runner and cause it to rotate. Finally, the generator converts the rotational energy into electricity. This concept of impulse turbines allows energy conversion with high efficiency throughout their operating range [2]. Hence, Pelton turbines are perfectly suited to stabilise the power grid efficiently for a wide range of electricity demand fluctuation amplitudes.

The Pelton turbine bucket is designed for particular impulse operating conditions, where a circular water jet shape of a certain diameter is assumed. The water jet quality, quantifying the actual to the design-assumed water jet shape, must be maintained so that the losses at the bucket are minimised to achieve a high-efficiency performance over a wide operating range. The efficiency can decrease by 0.5% to 2% with large water jet deformations and deviations [3, 4, 5]. A reduction of the mass flow rate can be realised by closing all spear valves equally or switching off individual nozzles. By reducing the number of operated nozzles, the water jet diameter can be kept close to the assumed diameter in the bucket design, and the buckets interact longer with the water jet. Thus, the regulation scenario with fewer nozzles in operation is commonly preferred, where rotational-symmetric configurations are chosen to distribute the runner axis loads evenly.

Because of the importance of the water jet quality on the Pelton turbine performance, many researchers considered the manifold in the prediction of the Pelton turbine efficiency [6, 7, 8].

Only a few works document the consideration of part-load analysis with a reduced number of open nozzles in Pelton turbine manifolds [9]. To improve the understanding of the implications of operating a reduced number of nozzles on the water jet quality, we numerically simulate the flow in a multi-nozzle Pelton turbine manifold, considering different nozzle operating conditions for even load distributions. The flow field established in the manifold is analysed, and the water jet quality is evaluated in terms of deviation and deformation.

2. Methodology and Setup

The geometry of the investigated Pelton turbine manifold is shown in Figure 1 (a). Six branch lines lead the flow from the manifold to the internally regulated nozzles, where the non-dimensional spear valve opening ratio s/d_0 is 0.79. The central spear body is held by vertically arranged profiles. The manifold inlet pipe has been extended upstream by a pipe of the length of five manifold inlet diameters. Cylindrical free-stream domains with a diameter of five times the nozzle exit diameter and a length of ten times the nozzle exit diameter are attached downstream of all open nozzle exits as indicated in Figure 1 (b).

The three-dimensional Navier-Stokes equations are solved using the Volume-Of-Fluid (VOF) approach to simulate the two-phase flow. The $k-\omega$ SST turbulence closure is employed to model turbulence. The local Euler time-stepping scheme is applied to obtain steady-state flow solutions. All gradient terms are evaluated with a cell value-limited least squares scheme. The divergence term in the volume fraction transport equation is calculated with the Van Leer limited Gauss scheme. A second-order upwind scheme is used to discretise all other divergence operations. A linear Gaussian scheme is used to solve all Laplace operations.

A fully structured mesh grid is used to discretise the computational domain with 14 (single nozzle) to 32 (all six nozzles) million hexahedral cells, where a detail is shown in Figure 1 (b). The mesh is refined towards all solid surfaces to guarantee $y^+ \leq 5$. Hahn et al. [10] showed by performing a grid sensitivity analysis that the utilised mesh resolution is sufficient to capture the main flow features. A hanging-node refinement is used in the region of the nozzle exit and the free water jet.

The total head of 80 m has been applied at the manifold inlet with a turbulence intensity of 5%. The hydraulic diameter is specified as the turbulent mixing length scale at the manifold inlet. Free-stream boundary conditions with standard ambient conditions have been set at the outlet and the free-stream domain. All solid surfaces are handled as no-slip walls.

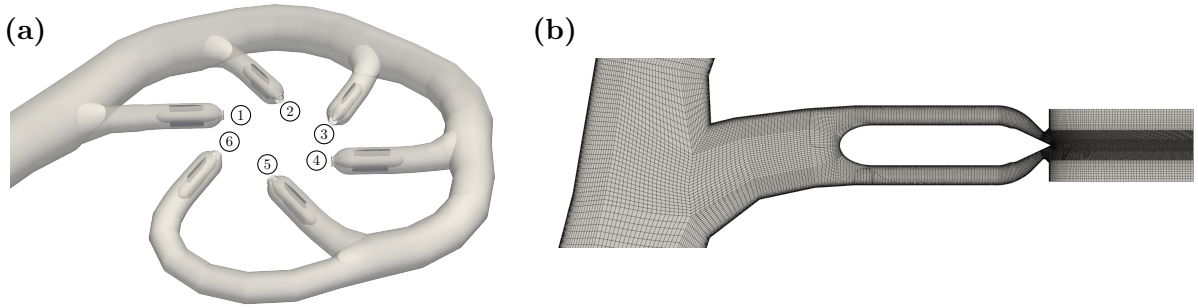

Figure 1. The investigated distributor manifold geometry is shown in (a), where the number of the individual nozzles is indicated. (b) shows a detail of the structured mesh with hanging-node refinement at the nozzle exit and the free water jet region.

Journal of Physics: Conference Series **2752** (2024) 012164 doi:10.1088/1742-6596/2752/1/012164

3. Results

The velocity magnitude contours are shown in Figure 2 for different nozzle operation configurations at the same spear-valve opening position. Clearly, the flow velocities are lower

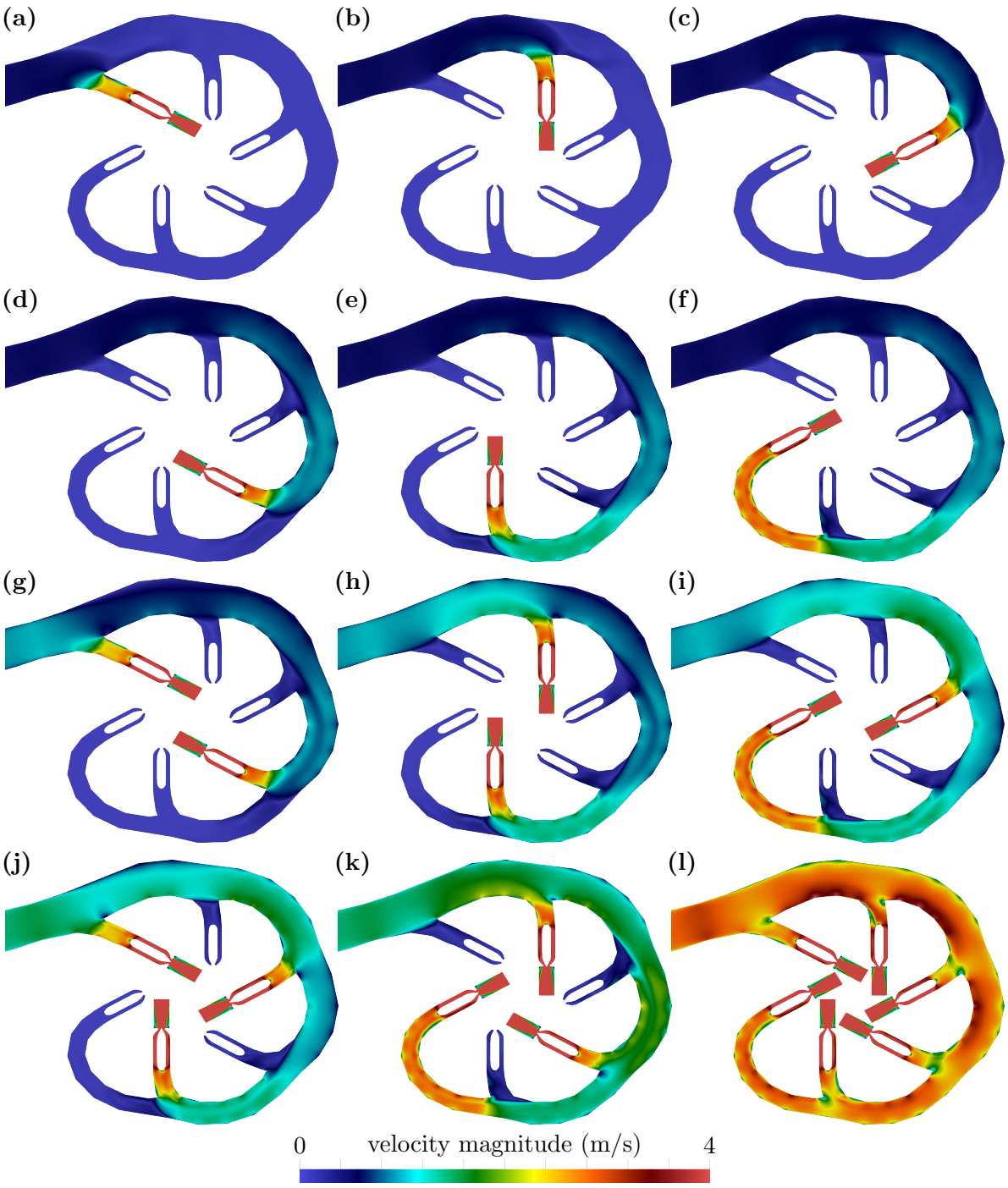

Figure 2. The velocity magnitude contours in the mid-plane view are shown for different active nozzle configurations; (a) to (f) single nozzle operation, (g) to (i) double nozzle operation, (j) and (k) triple nozzle operation, and (l) all six nozzles in operation.

Table 1. The area-averaged secondary velocities normalised by the primary velocity is tabulated in percent at a station upstream of the nozzles for individual operating conditions.

	①	②	③	④	⑤	⑥
single	8.24	10.85	10.95	10.68	12.12	9.53
double	7.40	10.82	10.38	9.91	12.30	9.33
triple	7.36	13.30	10.37	9.17	11.48	9.32
all six	7.86	17.76	11.54	9.05	8.94	9.69

in the manifold with a reduced number of active nozzles, while velocity magnitudes remain similar in the branch lines of all open nozzles. Thus, the inflow angles into the branch line are altered depending on the nozzle operating configuration. For example, Figure 2 (a) shows that the flow separates off the first branch line walls at the junction. This flow separation at the first nozzle reduces with double nozzle operation and diminishes entirely at the first nozzle with triple nozzle operation, as shown in Figures 2 (g) and (j), respectively. With all six nozzles in operation, Figure 2 (l) shows that the flow velocities are higher in the manifold, and the flow separation occurs in the branch line of the first nozzle on the opposite side as compared to the single nozzle operation. This flow field evolution with different numbers of nozzles in operation can be observed for several branch lines in Figure 2. Evidently, high flow velocities at the entrance of branch lines form at different locations depending on the number of nozzles in operation, which can cause the flow to separate at different locations.

The secondary velocity ratios, i.e. the area-averaged perpendicular flow velocity components normalised by the principal flow velocity component, have been related to the free water jet deformation and are caused by flow deviations into the branch lines. Therefore, the secondary velocity ratios are calculated at a station upstream of the nozzles, and the results are listed in Table 1 for the different nozzle operating conditions. The first nozzle exhibits particularly low secondary velocity ratios, while the second nozzle shows the highest secondary velocity ratio when all six nozzles are active. Clear statistical trends cannot be observed in Table 1. Rather the particular flow field at the branch line junction has to be analysed for the particular nozzle operating condition to understand the cause of the secondary velocity ratios.

The mass flow rate imbalances between the spear body holder sides are presented in Table 2, i.e. $(\dot{m}_l/(\dot{m}_r+\dot{m}_l))-0.5$ where the indices l and r denote the left and right side of the spear body holder, which can indicate the cause of the water jet deviation. The effect of the changing inflow angles into the first branch line with different numbers of nozzles in operation can be recognised in Table 2, which causes even a sign change for the first nozzle. A sign change does not occur for higher-numbered branch lines, but the trend of increasing values can be observed considering the

Table 2. The mass flow rate imbalance between the two sides of the vertically mounted spear valve holder is listed in percent for the nozzles at individual operating conditions.

	①	②	③	④	⑤	⑥
single	-0.43	0.35	0.37	0.40	0.60	1.43
double	-0.03	0.72	0.84	0.33	0.56	1.27
triple	0.34	1.15	0.79	0.84	0.52	1.32
all six	0.79	1.97	1.10	1.26	1.57	1.28

flow field implications shown in Figure 2. The flow at the fourth branch line junction is similar for the single and double nozzle operation because the manifold flow is hardly affected by the operation of upstream-located nozzles, see Figures 2 (d) and (g). When downstream nozzles are opened, see Figures 2 (k) and (l), the inflow angles at the fourth branch line junction change affecting the mass flow rate imbalances listed in Table 2 significantly.

Figure 2 reveals the generation of large-scale flow structures occurs for some nozzle operating conditions in the manifold. For example, the results of Dean-vortices can be observed when the third nozzle is closed and nozzles connected further downstream to the manifold are open. Figures 2 (d-f), (g-h), and (k) reveal a particular line of low-velocity magnitudes in the manifold starting upstream of the third nozzle. These vortical flow structures are the cause of small differences in the secondary flow ratios and the imbalances of the mass flow rates between the spear body holder sides. For example, Tables 1 and 2 exhibit for the fifth nozzle similar secondary velocity rations and similar mass flow rate imbalance values between the spear holder sides for single, double, and triple nozzle operation. Also, Figures 2 (e), (h), and (j) reveal a similar flow field at the fifth branch line junction, but the footprint of the upstream generated vortical

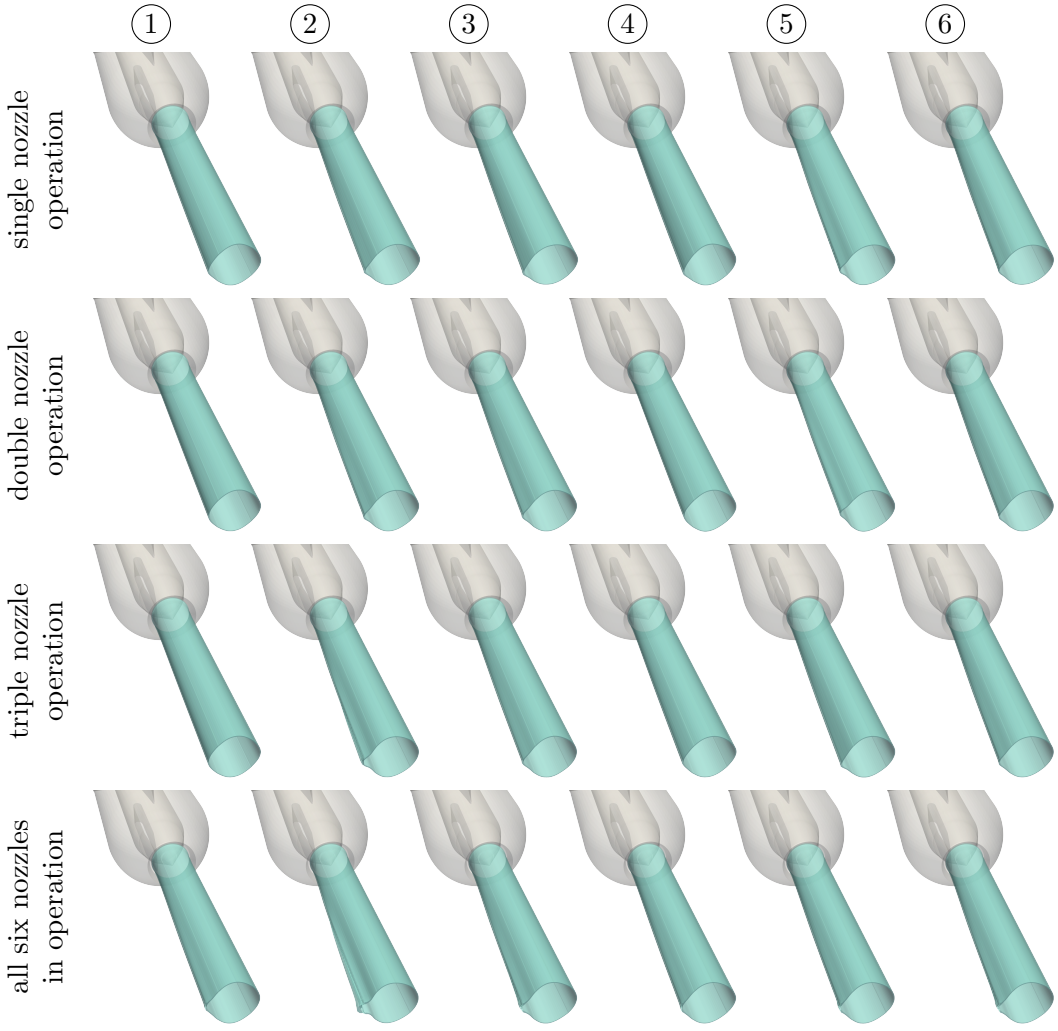

Figure 3. The water jet shape is illustrated by iso-surfaces for different active nozzle configurations.

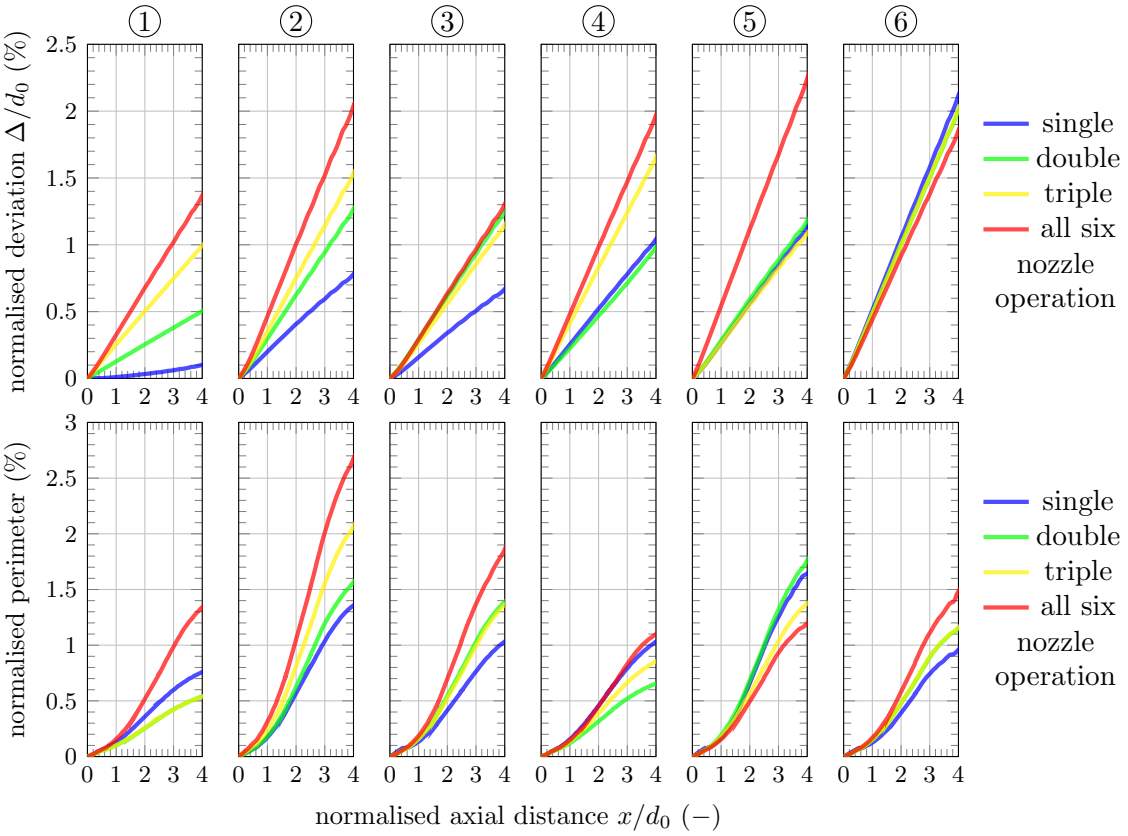

Figure 4. The top row shows the deviations of the water jet centreline off the nozzles axis normalised by the nozzle diameter as functions of the axial distance from the nozzle orifice. The water jet perimeters normalised by the circumference of the ideal circular water jet are plotted in the lower row as functions of the axial distance from the nozzle orifice.

structures has different strengths.

The water jet shapes at the different nozzle operating conditions are shown in Figure 3 in terms of iso-surfaces. The water jet shape deformations are generally dominated by Dean-vortices (and exhibit the typical shape reported in literature [11, 12]), which are forming due to the curvature of the branch lines. The comparison of the predictive parameters, i.e. secondary mass flow ratio and the imbalance of the mass flow rates between the spear body holder, with the water jet shapes shown in Figure 3 does not reveal straightforward relations.

The water jet qualities are quantified in Figure 4 showing the deviation off the centre axis and the ratio of the water jet perimeter to the ideal undistorted circumference. The water jet deviation is generally lower for single nozzle operation and higher when all nozzles are open. The best performance in terms of water jet deviation is achieved for the first nozzle at single nozzle operation, and the worst performance occurs at the fifth nozzle when all nozzles are operated. The worst water jet deformation occurs at the second nozzle when all nozzles are operated, while the lowest water jet deformation is achieved at the first nozzle with double and triple nozzle operation.

The first nozzle is the best choice for single nozzle operation, revealing the lowers losses, deviation, and water jet deformation. The combination of the first and fourth nozzles is best for double nozzle operation in all considerations. The best choice for triple nozzle operation is less straightforward because only the water jet deviation is clearly lower when the first, third, and

fifth nozzles are chosen. Assuming that the impact of the water jet shape deformation affects the Pelton turbine efficiency linearly, the first, third, and fifth nozzles perform best in triple nozzle operation.

4. Conclusions

Only a reduced number of nozzles are opened at the part-load operation of multi-nozzle Pelton turbines. This present contribution analysed the flow phenomena occurring at lower mass flow rate operating conditions in the Pelton turbine manifold using numerical flow simulations. The impact on the free water jet quality was evaluated and reported in terms of deviation and normalised perimeter. The main conclusions are as follows;

- With fewer nozzles in use, the velocities in the distributor manifold reduce compared to a configuration with all six nozzles in operation. Hence, flow angles at the branch line junctions change, affecting the water jet quality.
- Clear trends could not be observed between different nozzle operating conditions. Thus, all scenarios have to be simulated to guarantee an optimal choice of activated nozzles.
- Generally, better free water jet qualities were observed when the number of operating nozzles was reduced. However, the fifth water jet shape exhibited better performance parameters because the secondary velocities were reduced when all six nozzles were operated.
- The water jet deviation was observed to be similar for the final nozzle at all individual nozzle operating conditions. Thus, the nozzle orientation could be adjusted so that the free water jet emerges as intended by the bucket design.

Baffle blades are commonly used to improve the strength of the distributor at branch line junctions. Figure 2 (l) reveals stagnation points at the locations where baffle blades are commonly placed when all six nozzles are in operation, which suggests that baffle blade do not affect the internal flow. However, these stagnation points are not present for other nozzle operating conditions, and hence, deterioration of the flow field can be expected with baffle blades for conditions with less nozzles in operation. Perforations in the baffle blades might mitigate the impact of baffle blades on the flow field when a lower number of nozzles are operated. The final nozzle is expected to be less affected by baffle blades and hence, should be considered for single nozzle operation.

References

[1] Giesecke J and Mosonyi E 2009 *Wasserkraftanlagen: Planung, Bau und Betrieb* vol 5 (Springer-Verlag)
[2] Paish O 2002 *Renewable and sustainable energy reviews* **6** 537–556
[3] Staubli T and Hauser H 2004 *IGHEM2004, Lucerne, Switzerland* **1** 1–9
[4] Peron M, Parkinson E, Geppert L and Staubli T 2008 *International Conference on Hydraulic Efficiency Measurements, Milan, Italy, Sept* pp 3–6
[5] Santolin A, Cavazzini G, Ardizzon G and Pavesi G 2009 *Proceedings of the Institution of Mechanical Engineers, Part A: Journal of Power and Energy* **223** 721–728
[6] Jošt D, Mežnar P and Lipej A 2010 *IOP conference series: Earth and Environmental Science* vol 12 (IOP Publishing) p 012080
[7] Zeng C, Xiao Y, Luo Y, Zhang J, Wang Z, Fan H and Ahn S H 2018 *Renewable Energy* **125** 270–282
[8] Kumashiro T, Alimirzazadeh S, Maertens A, Jahanbakhsh E, Leguizamón S, Avellan F and Tani K 2019 *IOP Conference Series: Earth and Environmental Science* vol 240 (IOP Publishing) p 072006
[9] Florian H 2013 *Konstruktion und numerische Optimierung einer Verteilrohrleitung einer vertikalen sechsdüsigen Peltonturbine* Master's thesis TU Graz
[10] Hahn F, Semlitsch B and Bauer C 2022 *IOP Conference Series: Earth and Environmental Science* vol 1079 (IOP Publishing) p 012082
[11] Zhang Z and Casey M 2007 *Proceedings of the Institution of Mechanical Engineers, Part A: Journal of Power and Energy* **221** 1181–1192
[12] Riemann S 2009 *Untersuchung der instationären Strömung in einer Peltonturbine* Ph.D. thesis Technische Universität München